CO-oxidation model with superlattice ordering of adsorbed oxygen. I. Steady-state bifurcations

E. W. James, C. Song, and J. W. Evans

Citation: The Journal of Chemical Physics **111**, 6579 (1999); doi: 10.1063/1.479949
View online: http://dx.doi.org/10.1063/1.479949
View Table of Contents: http://scitation.aip.org/content/aip/journal/jcp/111/14?ver=pdfcov
Published by the AIP Publishing

CO-oxidation model with superlattice ordering of adsorbed oxygen. I. Steady-state bifurcations

E. W. James
Ames Laboratory and Department of Mathematics, Iowa State University, Ames, Iowa 50011

C. Song
Ames Laboratory, Iowa State University, Ames, Iowa 50011

J. W. Evans[a)]
Ames Laboratory and Department of Mathematics, Iowa State University, Ames, Iowa 50011

(Received 7 April 1999; accepted 14 July 1999)

We analyze a model for CO oxidation on surfaces which incorporates both rapid diffusion of adsorbed CO, and superlattice ordering of adsorbed immobile oxygen on a square lattice of adsorption sites. The superlattice ordering derives from an ''eight-site adsorption rule,'' wherein diatomic oxygen adsorbs dissociatively on diagonally adjacent empty sites, provided that none of the six additional neighboring sites are occupied by oxygen. A ''hybrid'' formalism is applied to implement the model. Highly mobile adsorbed CO is assumed randomly distributed on sites not occupied by oxygen (which is justified if one neglects CO–CO and CO–O adspecies interactions), and is thus treated within a mean-field framework. In contrast, the distribution of immobile adsorbed oxygen is treated within a lattice–gas framework. Exact master equations are presented for the model, together with some *exact* relationships for the coverages and reaction rate. A precise description of steady-state bifurcation behavior is provided utilizing both conventional and ''constant-coverage ensemble'' Monte Carlo simulations. This behavior is compared with predictions of a suitable analytic pair approximation derived from the master equations. The model exhibits the expected bistability, i.e., coexistence of highly reactive and relatively inactive states, which disappears at a cusp bifurcation. In addition, we show that the oxygen superlattice ordering produces a symmetry-breaking transition, and associated coarsening phenomena, not present in conventional Ziff–Gulari–Barshad-type reaction models. © *1999 American Institute of Physics.* [S0021-9606(99)70338-7]

I. INTRODUCTION

In recent years, a rich variety of nonlinear dynamics, steady-state bifurcation behavior, and spatial pattern formation, has been observed in catalytic surface reactions under ultrahigh vacuum conditions on single crystal substrates. Furthermore, suitably tailored mean-field rate equation and reaction–diffusion equation treatments have been extremely successful in elucidating this behavior.[1] However, it is well recognized that these treatments cannot precisely describe the influence of adlayer ordering on the reaction kinetics.[2] Furthermore, it was also recently noted that the conventional description of chemical diffusion used in reaction–diffusion equation treatments is overly simplistic. Diffusion of individual reactants in mixed adlayers is not independent, and ''interference effects'' may significantly affect chemical wave propagation.[3] Lattice-gas models can naturally address these complications. As a result, they have been invoked in an attempt to describe behavior in these reactive systems[4] with the same level of sophistication as applied to treat the equilibrium properties of unreactive adlayers.[5]

However, there have been two primary and common shortcomings of most previous lattice–gas model studies. First, there has been a general lack of appreciation of the important role of rapid surface diffusion of reactant species (at least some of which have hop rates many orders of magnitude greater than other relevant rates). This rapid mobility produces strong metastability and hysteresis in the reaction kinetics, and also controls the length scale of spatial pattern formation.[6–8] Many studies have completely neglected surface mobility, whereas in fact it is effectively the *hydrodynamic regime* of rapid surface mobility for these reaction models which is of physical relevance.[7–9] It should be noted that some ''hybrid'' models and simulation procedures have been developed to directly assess this regime.[7,8,10] Second, there has been little attempt to incorporate into lattice–gas models realistic adspecies interactions. These interactions produce significant adlayer ordering, and thus must strongly influence the reaction kinetics. A typical scenario is that there exist strong repulsive short-range interactions, and possibly weaker longer range interactions, between adspecies.[11] The former produce so called ''superlattice ordering'' (adopting surface chemistry terminology), which means that adspecies are locally ordered in a periodic array with unit cell larger than that of the array of adsorption sites.

As a result of these two shortcomings of previous modeling, we are motivated to develop a new ''canonical'' model for CO oxidation. This model introduces commonly

a)Electronic mail: evans@ameslab.gov

observed superlattice ordering of adsorbed oxygen,[11] and also incorporates very rapid diffusion of adsorbed CO. The former is achieved through a modified adsorption rule for O_2, which precludes the creation of neighboring pairs of adsorbed O (and which reflects the presence of very strong repulsive interactions between such adatoms). Although our model is still rather simplistic, ignoring other adspecies interactions, it does incorporate some basic features of real systems neglected in previous models, the consequences of which we discuss in detail in this paper. We forgo comparison with experiment here, as such comparison would benefit from further refinement of the model. However, we do note that our model has already been successfully applied to elucidate fluctuation behavior observed in CO oxidation on a nanoscale Pt field emitter tip.[12]

Our new ''canonical'' CO oxidation model is described in detail in Sec. II, together with its exact master equations, as well as some *exact* relationships which apply for the reaction rate and for the steady-state coverages. Simulation procedures and analytic approximations to the master equations are discussed in Sec. III. The basic properties of the model including its steady-state bifurcation and critical behavior are analyzed in detail in Sec. IV. Then, in Sec. V, we focus on a specific consequence of the introduction of superlattice ordering of adsorbed oxygen. We show that the reactive steady states of the model exhibits a symmetry-breaking order–disorder transition, akin to behavior in equilibrium models with superlattice ordering. We also observe a novel domain coarsening phenomenon associated with symmetry breaking, and analyze its kinetics. Finally, in Sec. VI, we summarize our findings.

II. REACTION MODEL

A. Langmuir–Hinshelwood mechanism and adlayer structure

In this study, we consider exclusively surfaces characterized by a square lattice of adsorption sites. We adopt a conventional Langmuir–Hinshelwood mechanism for CO oxidation as indicated below, where ''gas'' denotes a gas phase species, and ''ads'' an adsorbed phase species (see Fig. 1).

(i) CO(gas) adsorbs at single empty sites at rate P_{CO}, and CO(ads) desorbs at rate d;
(ii) O_2(gas) adsorbs dissociatively at diagonal nearest-neighbor (NN) empty sites at rate $\frac{1}{2}P_{O_2}$, *provided* that all six additional NN sites to these are unoccupied by O(ads). Furthermore, O(ads) does not desorb and is assumed immobile.
(iii) CO(ads) is assumed highly mobile (e.g., via rapid hops to NN and diagonal NN empty sites), and is assumed randomly distributed on sites not occupied by O(ads). This implies neglect of CO(ads)–CO(ads) and CO(ads)–O(ads) interactions.
(iv) Adjacent CO(ads) and O(ads) react at rate k.

Our prescription of oxygen adsorption is termed the ''eight-site rule'' since an ensemble of eight sites not occupied by O(ads) are required for adsorption. This rule was originally applied to describe dissociative adsorption of oxygen on Ni(100)[13] and Pd(100).[14,15] Together with the immobility of O(ads), this adsorption rule ensures that *no* adjacent pairs of O(ads) are created during the reaction process. As a result, the oxygen adlayer tends to display ''checkerboard'' or centered two-by-two $[c(2\times2)]$ ordering, especially for higher coverages of O(ads) (see Fig. 2). Such ordering in oxygen adlayers (in the absence of reaction) has indeed been observed experimentally for metal(100) surfaces including[11] Pd(100), Rh(100), Ni(100), Fe(100), and Cu(100), but not for Pt(100) where O(ads) displays more complicated superlattice ordering.[11] Both the eight-site rule and the appearance of $c(2\times2)$ ordering reflect the presence of strong NN O(ads)–O(ads) repulsive interactions.

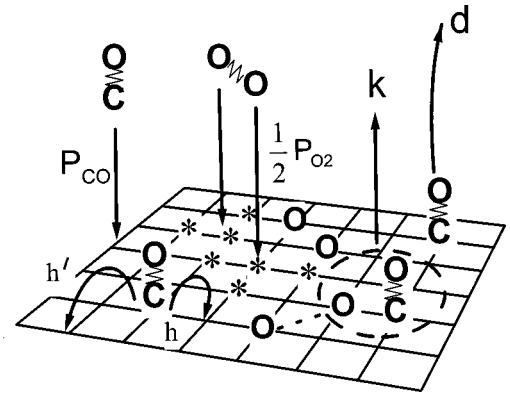

FIG. 1. Schematic of the CO oxidation model illustrating the various mechanistic steps, together with their rates. For the O_2 (gas) adsorption event, the eight sites required to be unpopulated by O (ads) are indicated by *. The dotted line between two O (ads) indicates that they were associated with the same molecule. CO (ads) is shown to hop to NN empty sites at rate h, and to next NN empty sites at rate h', where in our model both $h\to\infty$ and $h'\to\infty$ (but h'/h can have any limiting value).

As indicated in Sec. I, superlattice ordering has not been incorporated into most previous lattice–gas modeling of CO oxidation. In these models, oxygen adsorption was assumed to occur on adjacent (NN) empty sites,[4,6–9,16] and, consequently, the coverage of oxygen could increase up to 1 monolayer (ML). As a result, the steady states of these reaction models exhibit an unphysical ''oxygen poisoning tran-

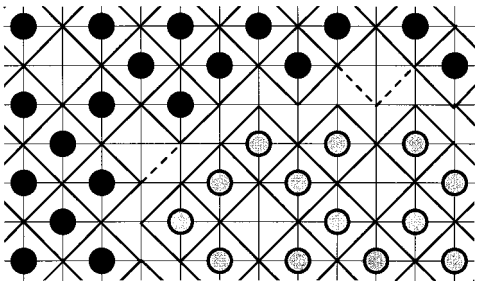

FIG. 2. Schematic of the configuration of oxygen atoms in a jammed state. Atoms in two adjacent $c(2\times2)$ domains of different phase are indicated by black and gray circles. Also shown is the hard-square representation where atoms are replaced by diamonds. This representation highlights both the three internal defects or holes, as well as the domain boundary which is decorated by two external defects (indicated by dashed lines). The hard-square representation will be used in some subsequent figures, shading diamonds in one phase by black, and those in the other by gray.

sition'' to a state where the surface is covered by 1 ML of oxygen. Among previous studies, we mention two exceptions, which did incorporate the eight-site rule. Reference 12 reported briefly some properties and consequences of coverage fluctuations in the above model near a cusp bifurcation or critical point. Reference 17 considered some aspects of model behavior for *instantaneous* reaction ($k=\infty$), with large hop rates for CO(ads). In this case, a CO(ads) reacts instantaneously with the first O(ads) that it meets (which is more likely located at a protrusion rather than an indentation at oxygen islands edges). Also, the coverage of CO(ads) is negligible. Our model is different reflecting the feature that the hop rates are far larger than all other rates (including k). This implies that CO(ads) is uniformly distributed with a significant coverage, and reacts with equal probability with all O(ads) species.

Next, we introduce the *standard notation* for monomer–dimer or $A+B_2$ surface reaction models of CO oxidation, of which our model is one example. This notation will be used throughout the rest of the paper. Then, we discuss further the model parameters, and our assignment of their values. In this notation, one denotes the ''monomer'' CO by A, and the ''dimer'' O_2 by B_2 (and O by B), so the overall reaction mechanism becomes $A+\frac{1}{2}B_2 \rightarrow AB$. Then, P_{CO} becomes P_A, and P_{O_2} becomes P_{B_2}. Note that P_A corresponds to the impingement rate per site for A(gas). Also, since there are two diagonal NN pairs of sites for each single site on the square lattice, P_{B_2} corresponds to the impingement rate per site for B_2(gas). Below, we choose $P_A+P_{B_2}=1$ (which sets the time scale), and often describe behavior as a function of $P_A=1-P_B$. We also set $k=1$ when presenting specific results. The coverage of CO(ads) or A(ads) is denoted by [A], and that for O(ads) or B(ads) by [B], so the total coverage is given by $\theta=[A]+[B]$ (where these quantities are measured in units of monolayers).

Finally, we briefly comment on and illustrate some basic features of the ordering in the B adlayer. Ordering is analogous to that in an equilibrium ''hard-square model,'' where adspecies B have infinitely repulsive NN interactions.[18] As shown in Fig. 2, $c(2\times 2)$ domains have degeneracy two, atoms in domains of different phase residing on one of two interpenetrating ''sublattices.'' (The latter terminology is adopted from equilibrium statistical mechanics, although it is potentially confusing here as adspecies populating a sublattice exhibit superlattice ordering!) In addition, individual domains can have ''internal defects'' or ''holes'' H, that is sites *not* occupied by B(ads) which are surrounded by four diagonal adjacent B(ads). The ''coverage'' of density (per site) of these holes is denoted by $[H]$.

A schematic ''hard-square representation'' of the B adlayer, highlighting these features, replaces the circular B adspecies by diamonds with side length $\sqrt{2}$ times the lattice constant. This representation is particularly useful in characterizing so called ''jammed states,'' where there are no ensembles of sites available for further adsorption of B_2(gas). In such states, the only uncovered regions of the surface correspond to either isolated internal defects, or to domain boundaries that separate adjacent domains of different phase. The latter are diagonal strips of width $1/\sqrt{2}$, occasionally decorated by isolated ''external'' defects (see Fig. 2). Thus, in the hard-square representation, the fractional area F of domain boundary in jammed states satisfies

$$F=1-2[B]-2[H] \tag{1}$$

B. Exact master equations and results

Despite the feature that our model incorporates nontrivial spatial correlations in the distribution of adsorbed B's it is possible to write down a formally *exact* hierarchy of master equations describing the reaction kinetics and the evolution of the local ordering. For convenience, below we drop the ''ads'' when referring to adsorbed A or B. We let E denote empty sites, and Z denote sites *not* occupied by B. So one could write $E=\text{not(A or B)}$, and $Z=\text{not(B)}$. Extending the notation of Sec. II A, we let $[K]$ denote the fraction of sites in state $K=$A,B, E, or Z. Then, from conservation of probability, one has that

$$[E]=1-[A]-[B], \quad \text{and} \quad [Z]=1-[B]. \tag{2}$$

Also, we let $[KJ]$ denote the probability that the left site in a specific NN pair is in state K, and the right one is in state J, etc. Then, from conservation of probability, one has that, e.g.,

$$[ZZ]+[BZ]+[ZB]+[BB]=1, \tag{3}$$

where $[B\,B]=0$ and $[B\,Z]=[Z\,B]=[B]$, so $[Z\,Z]=1-2[B]$. Similar notation is adopted for probabilities of configurations of various larger sets of sites.

Using this notation, the exact master equations for the coverages [A] and [B] have the form (cf. Ref. 7)

$$d/dt\ [A]=P_A[E]-d[A]-4k[AB], \tag{4a}$$

and

$$d/dt\ [B]=2P_{B_2}\begin{bmatrix} & & Z & \\ & Z & E & Z \\ Z & E & Z & \\ & Z & & \end{bmatrix}-4k[AB]. \tag{4b}$$

The gain terms in these equations correspond to adsorption, with the eight-site rule reflected in the configuration probability which appears in Eq. (4b). The common loss terms due to reaction includes the probability [A B] for an adjacent AB pair, rather than the (incorrect) factored form [A][B]. The factor of 4 in these terms corresponds to the coordination number of the square lattice. There is also a loss term due to A desorption in Eq. (4a). Further simplification of the multisite configuration probabilities in Eq. (4) is possible exploiting the feature of our model that the A's are randomly distributed on Z sites. In particular, one has (cf. Ref. 7)

$$[AB]=([A]/[Z])[ZB]=[A][B]/(1-[B]), \tag{5}$$

providing an *exact* expression in terms of coverages for the reaction rate terms appearing in Eq. (4). The possibility of obtaining a simple exact expression for the reaction rate in this model is perhaps not surprising. It derives from the feature that every B is surrounded by exactly four Z sites, and

all Z sites are occupied by A with the same probability. For the configuration probability appearing in the adsorption term in Eq. (4b), simplification is again possible since the A's are randomly distributed on Z sites to obtain

$$\begin{bmatrix} & & Z & \\ & Z & E & Z \\ Z & E & Z & \\ & Z & & \end{bmatrix} = ([E]/[Z])^2 \begin{bmatrix} & & Z & \\ & Z & Z & Z \\ Z & Z & Z & \\ & Z & & \end{bmatrix}. \tag{6}$$

There is no simple exact expression for the configuration of eight Z's appearing on the right hand side (RHS) of Eq. (6). Thus, Eq. (4) should be regarded as the lowest order equations in a hierarchy of equations for the probabilities of various multisite configurations. However, in Sec. III, we shall discuss possible approximations for Eq. (6), which allows closure of the basic rate equations (4).

Finally, we note one important consequence of the exact expression, Eq. (5), for the reaction rate. If one considers the steady state, where $d/dt\ [K]=0$ for $K=$A or B, then from Eqs. (4a) and (5), one obtains

$$[\mathrm{A}] = \frac{P_\mathrm{A}(1-[\mathrm{B}])}{P_\mathrm{A}+d+4k[\mathrm{B}]/(1-[\mathrm{B}])}. \tag{7}$$

Thus, there is a simple exact relationship between the steady-state values of [A] (corresponding to the CO coverage) and [B] (corresponding to the O coverage).

C. Special case $P_\mathrm{A}=0$ (eight-site model for B_2 dimer adsorption)

When $P_\mathrm{A}=0$ (so $P_{\mathrm{B}_2}=1$), there is no A adsorption. Thus, the process simply involves nonreactive irreversible adsorption of B_2 dimers, subject to the eight-site rule described in Sec. II A (ii), to form a immobile adlayer with $c(2\times2)$ short-range order. Adsorption will continue until there are no further available ensembles of eight empty sites suitable for adsorption, after which the system remains in a nonequilibrium ''jammed state.'' These types of nontrivial adsorption processes have been studied extensively within the framework of random sequential adsorption (RSA).[19] Of particular interest in these models is the dependence on coverage θ (=[B] here since [A]=0) of the ''sticking probability'' $S(\theta)$ that an impinging molecule will actually adsorb and remain on the surface. In general, it is possible to develop formally exact expansions for the short-time or low-coverage adsorption kinetics, and thus for $S(\theta)$. It is also possible to determine the precise way in which $S(\theta)$ vanishes on approaching jamming.

The RSA problem corresponding to our model with $P_\mathrm{A}=0$ has been studied extensively.[15] The coverage of the jammed state, $\theta_J=0.3616$, is well below the maximum value of 0.5 for perfect $c(2\times2)$ ordering. This jammed state is a collection of $c(2\times2)$ domains, containing ''internal defects'' or holes H the density of which equals $[H]=0.0098$,[20] separated only by domain boundaries which, from Eq. (1), have a fractional area (in the hard-square representation) of $F=0.2572$ (cf. Sec. I A). It also follows that $S(\theta)$ equals the probability appearing in Eq. (6) (noting that $[E]=[Z]$, when $P_\mathrm{A}=0$ and [A]=0). One can show that

$$S(\theta)=1-6\theta+(135/16)\theta^2+\mathrm{O}(\theta^3),$$

and (8)

$$S(\theta)\sim(\theta_J-\theta)/4, \quad \text{as} \quad \theta\to\theta_J,$$

from which a uniformly accurate Padé approximation can be constructed.[15] A detailed characterization of the disordered geometry of the jammed state is also available.[15]

III. METHODS OF ANALYSIS

A. Hybrid simulation procedures

Conventional kinetic Monte Carlo simulation of the above model with specified rates (for adsorption, desorption, and reaction) is possible with only minor modification to account for the randomly distributed, mean-field nature of the A. Specifically, for the B, one performs a conventional simulation tracking the position of every particle on the lattice. However, for the A, one simply tracks the total number of adsorbed particles. From this and the number of Z sites (not occupied by B), one can calculate the instantaneous probability that any Z site is occupied by A. This probability is then used in determining whether specific adsorption, desorption, and reaction events take place (see Ref. 7 for further discussion).

One feature of hybrid models, contrasting lattice–gas models with finite adspecies mobility,[21] is that they display bistability, i.e., there is a range of model parameters for which two stable steady states coexist.[7,8] This feature, familiar from conventional mean-field studies,[1] is illustrated explicitly in the figures in Sec. IV. It derives from the effective infinite mobility (and randomization) of the A's. The standard scenario in systems displaying bistability is that the attractive basins associated with two such stable states are separated by an unstable state. This unstable state is as easily determined as the stable states in mean-field models. However, in our hybrid reaction model, the unstable state incorporates nontrivial spatial correlations. Furthermore, it cannot be accessed by conventional simulation techniques. Fortunately, one can apply an unconventional constant-coverage ensemble simulation approach[22] to resolve this problem.[7] Here, one specifies some ''target'' coverage [A]* of A, for example, and performs a conventional simulation, except for the adsorption step. In that step, instead of adsorbing with fixed relative probabilities, one attempts to absorbs A if [A]<[A]*, and attempts to adsorb B_2 if [A]>[A]*. Then, one tracks the fraction of attempts to deposit A, and identifies the asymptotic long-time value of this fraction as the P_A corresponding to [A]*. These simulations recover the stable states obtained by conventional simulations, but also map out the connecting unstable states, thus allowing complete determination of the ''phase diagram.''

B. Pair approximation

To close the rate equations (4) at the lowest level, one needs a reasonable approximation for the eight-site configuration probability appearing on the RHS of Eq. (6) in terms

of the adspecies coverages. One can invoke the standard pair or Kirkwood-type approximation which has the form (cf. Ref. 7)

$$\begin{bmatrix} & & Z & \\ & Z & Z & Z \\ Z & Z & Z & \\ & Z & & \end{bmatrix} \approx [ZZ]^8/[Z]^8 = (1-2[B])^8/(1-[B])^8. \tag{9}$$

Then, inserting Eqs. (5), (6), and (9) into Eq. (4) produces a closed pair of equations for [A] and [B]. Here, we focus on the steady-state behavior predicted by these equations, which when using Eq. (7) to express [A] in terms of [B], follows from solving a high-order polynomial equation for [B]. See Appendix A for more details.

There is no reason to expect that the pair approximation, Eq. (9), will be particularly accurate for higher coverages of B. The simplest illustration of this inaccuracy is that for the RSA problem corresponding to $P_A=0$, this pair approximation predicts a coverage for the jammed state of $\frac{1}{2}$, rather than the nontrivial value of 0.3616. Furthermore, we shall see in Sec. V that the predictions for small P_A are also qualitatively incorrect. This failure derives in part from the feature that the pair approximation does not account for an observed dramatic symmetry-breaking feature of the reaction model for higher [B]. This symmetry breaking entails the development of unequal populations of B on the two sublattices associated with $c(2\times2)$ ordering. The pair approximation can be refined to account for symmetry breaking,[23] and a simple analysis is possible if only one sublattice is populated,[24] however such analyses still do not yield accurate results. See Sec. V for further discussion.

IV. STEADY-STATE PHASE DIAGRAM

A. Pair-approximation predictions versus exact behavior ($k=1$)

We shall see below that both the analytic pair approximation and the ''exact'' simulations consistently predict the following behavior. For sufficiently low $d<d_c$, the reaction model exhibits bistable steady states for a range $P^-<P_A<P^+$, where $P^\pm=P^\pm(d)$ denotes upper and lower saddle-node bifurcations or ''spinodals.'' (One exception is for $d=0$, where $P^-=0$ corresponds to a transcritical bifurcation.) Specifically, in the bistable region for $d<d_c$, a reactive stable state with low [A] (and high [B]) *coexists* with a relatively inactive stable state with high [A] (and low [B]). These two states are ''connected'' by an unstable state. The width, P^+-P^-, of the bistable region vanishes as $d\to d_c$ from below, where $d=d_c$ corresponds to a cusp bifurcation or ''critical'' point. We recall that conventional monomer–dimer or $A+B_2$ reaction models, with adsorption of immobile B_2 dimers onto *adjacent* empty sites, display a continuous B poisoning transition for lower P_A, both when A is immobile,[4,16] and infinitely mobile.[7] In contrast, obviously our model necessarily has $[B]\leqslant 1/2$, and thus cannot B poison, a feature consistent with the lack of oxygen poisoning in experimental observations.[1]

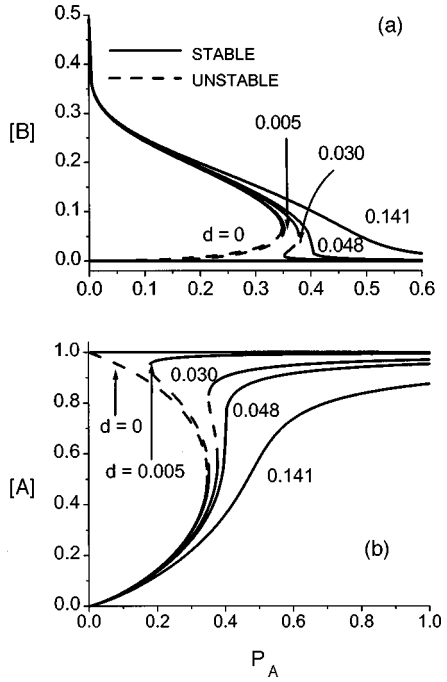

FIG. 3. Steady-state phase diagram predicted by the pair approximation showing the variation with P_A of: (a) [B]; and (b) [A] for various fixed d (shown) and $k=1$. Stable (unstable) steady states are indicated by solid (dashed) lines. Recall that [B] and [A] correspond to the coverages of O (ads) and CO (ads), respectively, and P_A to the impingement rate for CO (gas).

First, we present results for the steady-state phase diagram obtained from an analytic treatment using the pair approximation Eq. (9). Solving the polynomial equation in Appendix A produces the steady-state variation of [B] vs P_A shown in Fig. 3(a), for various d. The corresponding behavior of [A] obtained from Eq. (7) is shown in Fig. 3(b). For $d=0$, the bistable region extends from $P^-=0$ to $P^+\approx0.3481$. The cusp bifurcation at $d_c\approx0.048$ is apparent in Figs. 3(a) and 3(b) and, as $d\to d_c$, both P^- and P^+ approach $P_c\approx0.4004$. Note that for all values of d, one has $\frac{1}{2}-[B]\sim\text{const}(P_A)^{1/8}$, as $P_A\to0$, as shown in Appendix A.

Second, we present ''exact'' results for the steady-state phase diagram obtained using the constant-coverage simulations to access the unstable as well as the stable states. Figure 4(a) shows the behavior of [B] vs P_A, and Fig. 4(b) shows the behavior of [A] vs P_A, for various d. The behavior of these two quantities is related exactly by Eq. (7). For $d=0$, the bistable region extends from $P^-=0$ to $P^+\approx0.360$. One now finds a cusp bifurcation at $d_c\approx0.053$, a value slightly above the prediction from the pair approximation. As $d\to d_c$, both P^- and P^+ approach $P_c\approx0.414$.

Certainly, the general behavior predicted by the pair approximation agrees qualitatively with exact results. This is also evident in a different comparative representation of the steady-state phase diagrams in the (P_A,d) plane shown in Fig. 5. A more complete comparison of exact properties at the cusp bifurcation, and predictions from the pair approximation is given in Table I. See also Refs. 12 and 23. The one major difference is evident, specifically the nontrivial exact limiting behavior of $[B]\to0.4253$, as $P_A\to0$, in contrast to

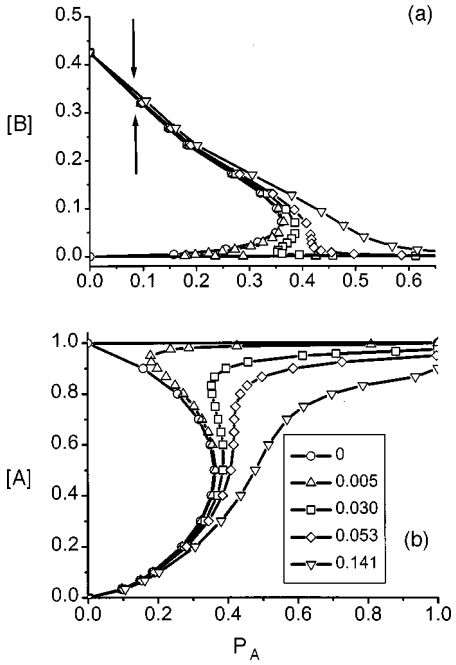

FIG. 4. Steady-state phase diagram predicted by constant-coverage ensemble simulations showing the variation with P_A of: (a) [B]; and (b) [A] for various fixed d (shown in the legend), and $k=1$. The arrows in (a) indicate the location of the symmetry-breaking transition. Recall that [B] and [A] correspond to the coverages of O (ads) and CO (ads), respectively, and P_A to the impingement rate for CO (gas).

the prediction of $[B]\to 1/2$ in the pair approximation. Note that the ''exact'' limiting behavior also differs from the RSA result that $[B]=0.3616$ for $P_A=0$. There is actually another more subtle difference between approximate and exact behavior, not evident by comparing Figs. 3(a) and 4(a). In conventional simulations of model behavior, as one decreases P_A (so [B] increases), one finds a symmetry-breaking transition in the reactive steady state, i.e., the populations of B on the two $c(2\times 2)$ sublattices become unequal. This transition and the limiting behavior as $P_A\to 0$ are discussed in some detail in Sec. V.

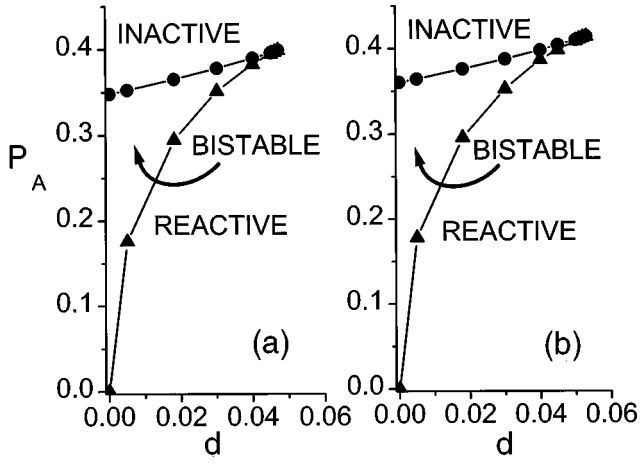

FIG. 5. Steady-state phase diagrams in the (P_A,d) plane showing the regions with a single reactive and (relatively) inactive state, as well as the bistable region obtained from: (a) the pair approximation; (b) simulations.

TABLE I. Comparison of ''exact'' properties at cusp bifurcation, and predictions from the pair approximation.

	d_c	P_c	[B]	[A]
Pair approximation	0.048	0.400	0.030	0.676
''Exact'' simulation	0.053	0.414	0.033	0.663

Finally, we comment on one other fundamental issue for systems such as our reaction model which exhibit bistability. One is naturally motivated to consider the relative stability of coexisting stable states, and in particular to determine the point of equistability (which should occur somewhere in the ''middle'' of the range of bistability).[7,8] This is akin to providing a Maxwell construction for a van der Waals-type phase diagram in an equilibrium system. The appropriate strategy to address this nontrivial issue is presented in Appendix B.

B. Steady-state dependence on reaction rate (k)

Since the above choice of $k=1$ is somewhat arbitrary, here we briefly discuss the dependence of steady-state behavior in our reaction model on the reaction rate k. As one might expect, there is no qualitative difference in the phase diagram for different k, and it can in fact be shown that behavior as $P_A\to 0$ is independent of k. However, there are some systematic trends which can be readily elucidated. To this end, it is most convenient to focus on the special case $d=0$, which has the broadest bistable region, $0\leqslant P_A\leqslant P^+$. Here, we write $P^+=P^+(k,d=0)=P^+(k)$. Some discussion of the general case where $d\geqslant 0$ is provided in Appendix C.

First, consider the regime where $k\ll 1$ (for $d=0$). Starting with an empty surface, one expects that, in this regime, the surface will almost completely fill on a time scale of order unity. Thereafter, each ''slow'' reaction event creates an empty pair of sites which are inevitably filled by A's, since the high coverage inhibits adsorption of B_2 dimers. Thus, one concludes that the surface will eventually become nearly poisoned with A's. This claim is consistent with Eq. (6) for $d=0$ and $k\ll 1$. This observation implies that $P_{s+}(k)\to 0$, as $k\to 0$.

Second, consider the regime where $k\gg 1$ (for $d=0$). Rapid reaction, together with the infinite diffusion rate for A in our hybrid model, implies that only one type of species can populate the surface (cf. Refs. 9, 17, and 25). In the reactive state, only B populates the surface, so $[B]>0$ and $[A]=0$. In this state, [B] decreases to zero, as P_A increases to P^+. The adsorption rate for A of $P_A(1-[B])$ approaches P_A, and the adsorption rate for B approaches $2P_B$, as $P_A\to P^+$ and $[B]\to 0$ (where rates are in terms of adspecies per site per unit time). Since these rates must be equal, it follows that $P_A=2P_B=2/3=P^+$, a value which reflects the stoichiometry of the reaction.

In summary, we conclude that $P^+(k)$ increases from 0 to 2/3, as k increases from 0 to ∞, passing through a value of 0.360, when $k=1$ (see Sec. IV A).

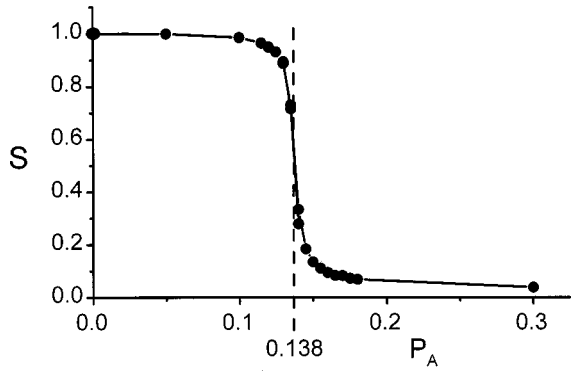

FIG. 6. Variation of the order parameter S with P_A in the reaction model with $d=0$. Results are shown for a 100×100 site lattice.

V. BEHAVIOR FOR LOW P_A: SYMMETRY BREAKING AND COARSENING

A. The symmetry-breaking transition

For $d=0$, we find that there is a spontaneous symmetry breaking in the reactive steady state of the model (i.e., the populations of B on the two $c(2\times2)$ sublattices become unequal) as P_A decreases, or [B] increases above a critical value. This feature ''replaces'' an unphysical oxygen or B poisoning transition familiar in conventional reaction models with dimer adsorption on adjacent sites.[4,16] To quantify symmetry breaking, we labeled the two $c(2\times2)$ sublattices by + and −, and let $[B_+]$ and $[B_-]$ denote the fraction of sites on the + and − sublattice occupied by B, respectively, so $[B]=([B_+]+[B_-])/2$. Then, we introduce the order parameter

$$S=|[B_+]-[B_-]|/([B_+]+[B_-]), \tag{10}$$

which naturally measures the imbalance in the $c(2\times2)$ sublattice populations of B. For an extremely large system, S should be negligible above the transition where there is no symmetry breaking, and should increase quickly below the transition achieving a value of near unity for small P_A. For smaller systems, this nonanalytic behavior is smoothed out. Figure 6 shows our simulation results for a 100×100 site system, where S increases quickly from a small but nonvanishing value (on the order of the inverse square root of the system size) to around unity, as P_A decreases below about 0.138. Thus, we identify the location of the transition as $P_A\approx0.138$ (±0.003), corresponding to $[B]\approx0.29$ (±0.02). No doubt, symmetry breaking also occurs for cases with $d>0$, when [B] increases above a value of about 0.29 (±0.03).

This behavior is entirely analogous to that at a symmetry-breaking order–disorder transition in an equilibrium system. A natural comparison is with the equilibrium hard-square model, which can be described as B's randomly occupying sites on a square grid subject to NN exclusion (as a result of infinite NN repulsions). In this model, the symmetry-breaking transition occurs when [B] increases above about 0.368.[18] The feature that the transition value of [B] in the hard-square model is substantially higher than in the reaction model is easily understood: the maximum value of [B] in the hard-square model is 0.5, versus a maximum reactive steady-state value of 0.4253, as $P_A\to0$ in the reaction model. In the latter case, the typically much higher density of internal defects within individual $c(2\times2)$ domains induces the symmetry-breaking transition at a correspondingly lower value of [B]. In future work,[23] we shall present a more detailed analysis of the transition in the reaction model, determining its universality class.

Finally, we note that if one starts with a system in a symmetric state (e.g., an empty surface), the evolution to a symmetry-broken state occurs via ''domain coarsening,'' just as for equilibrium systems.[26] Specifically, starting with an empty surface, the coverages of A and B quickly increase and stabilize. Thereafter, domains which are B rich on the + and − sublattices form, and grow in size. In Sec. V B, we consider this process for one special case. Both the coarsening process and the symmetry-breaking feature of the steady-state should be observable in reaction systems, just as in equilibrium systems, from the features of the $c(2\times2)$ ''superlattice spot'' in the low energy electron diffraction pattern.[27]

B. Evolution in the regime $P_A\to0+$

Next, we focus attention on the nontrivial limiting behavior of the reaction model for $P_A\ll1$. Consider the evolution of the model starting with an initially empty surface. If P_A is negligible (compared to $P_{B2}\approx1$), then initially B_2 dimers are deposited (effectively in the absence of A) according to the eight-site rule until the lattice is ''jammed'' with B at a coverage of about $[B]\approx0.3616$. At this point, a second much slower stage of the process commences mediated by ''slow'' deposition of A at a rate P_A, and thus characterized by a time scale $t'\propto P_At$. The effect of the slow deposition of A is the slow removal of individual B's, followed by the effectively immediate filling (measured on the time scale t') by B_2 dimers at any eight-site ensembles thus created. More specifically, removal of a single B by reaction in a jammed state with no eight-site ensembles may result in the creation of zero, one, or possibly more eight-site ensembles suitable for dimer adsorption. If none are created, the process continues by random removal of another B. If one is created, it is immediately filled by a dimer. If more than one is created, one is chosen at random and filled by a dimer (and we note that this leaves no further eight-site ensembles available for filling). Thus, the system evolves through a sequence of jammed states, with the characteristics described previously in Sec. II A.

From the above discussion, it is clear that one can directly simulate the limiting behavior as $P_A\to0+$ (on a time scale $t'\propto P_At$). We now report the results of such simulations. We start each simulation run with an initially jammed state, obtained from dimer filling according to the eight-site rule. Implementing the above dynamics, one finds that [B] initially decreases from the initial value of 0.3616. This corresponds to an initial increase in the density of internal defects within the individual $c(2\times2)$ domains from the initial value of $[H]=0.0098$, and ensuing stabilization at a value of 0.074 66. Subsequently, on a somewhat slower time scale, [B] starts to increase again as a result of the coarsening of

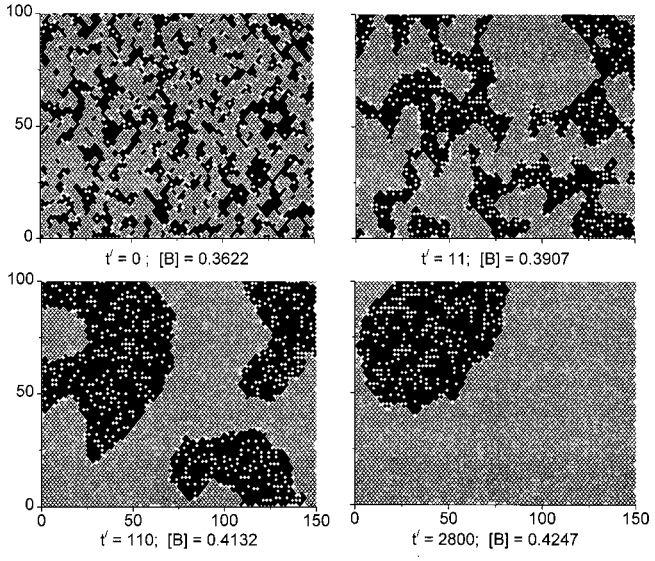

FIG. 7. Snapshots (using the hard-square representation) of a time sequence of B adlayer configurations for $P_A=0+$, which reveals the coarsening process. Corresponding times ($t' \propto P_A t$) and coverages ([B]) are indicated.

individual $c(2\times2)$ domains, finally reaching a value of 0.425 34. This coarsening process produces a decrease in the fractional area of domain boundary, $F=1-2[\mathrm{B}]-2[H]$. Evolution of the B adlayer during this coarsening process is illustrated in the sequence of snapshots in Fig. 7. We have determined the decrease of F with time t' for an 800×800 lattice. The results shown in Fig. 8 indicate that

$$F\sim(t')^{-0.47} \quad \text{for } 15<t'<250, \tag{11}$$

suggesting that for an infinite lattice one has $F\sim(t')^{-1/2}$, as $t'\to\infty$. Finally, we note that the characteristic linear dimension (or chord length) of $c(2\times2)$ domains scales inversely with F, and thus increases like $(t')^{1/2}$.

The latter behavior is reminiscent of classic Lifshitz–Cahn–Allen interface-curvature-driven coarsening.[26] Indeed, it is not unreasonable that the mean propagation velocity for domain boundaries in our model should scale with curvature, noting that the velocity vanishes for zero curvature. To illustrate this feature, in Fig. 9 we have shown the individual

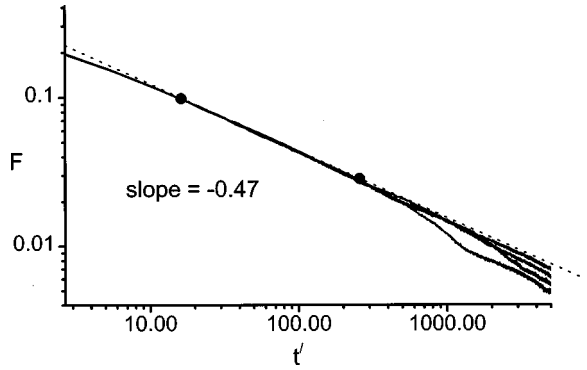

FIG. 8. Log–log plot revealing the decrease with time t' of the fractional area of domain boundary, F, averaged over four simulations on an 800 $\times$800 site lattice. The large dots indicate the regime from which we extracted the temporal scaling exponent listed in Eq. (11).

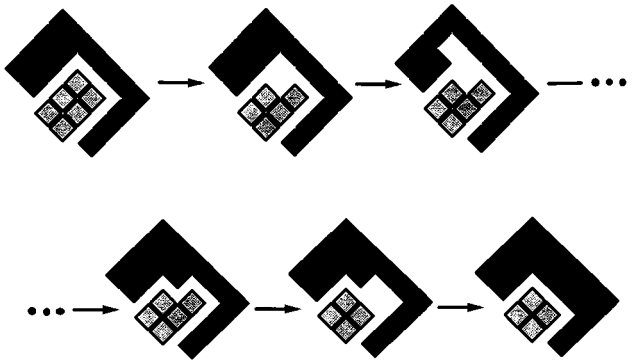

FIG. 9. Schematic (using the hard-square representation) of the shrinkage of a highly curved portion of domain boundary. In this sequence, a total of three B monomers are removed by reaction, and two B_2 dimers adsorb, yielding a net increase of one adsorbed B.

atomic steps in one pathway leading to the shrinkage by one lattice constant of a highly curved portion of domain boundary, and an associated increase in the number of adspecies. One can easily confirm that more steps are required for the similar shrinkage of a less curved portion of domain boundary. Finally, it is appropriate to note that various other nonequilibrium growth or evolution models,[28] and reaction models,[6,29] are described by Kardar–Parisi–Zhang or Edwards–Wilkinson equations, where interface propagation also has a curvature dependence.[28]

A modified (and more efficient) analysis of some aspects of behavior when $P_A\to0+$ exploits the feature that eventually a single sublattice is populated (in a finite system). It is thus natural to instead start the simulation with a perfect $c(2\times2)$ ordered state, where $[H]=0$. The dynamics then involves with random monomer removal, followed if possible by immediate dimer adsorption, but with these processes *restricted* to one sublattice. In this case, we find that the coverage [B] decreases monotonically from 0.5, eventually stabilizing at the value of 0.425 34. Correspondingly, $[H]=1/2-[\mathrm{B}]$ (since $F=0$) increases monotonically, eventually stabilizing at 0.074 66. These results are consistent with those above. We should note that it is also possible to develop an analytic master equation formalism for this sublattice B dynamics, which occurs on the time scale t'.[30]

C. Direct analysis of steady-state behavior when $P_A\to0+$

It is possible to develop a *direct* analysis for the (long-time) steady-state adlayer structure in the regime $P_A\to0+$. This steady state is in a dynamic equilibrium involving desorption of B monomers, and adsorption of B_2 dimers, with the simplifying feature that this dynamics is restricted to one sublattice. (See the discussion at the end of Sec. V B, and recall that $S=1$ in this regime.) We assume that the + sublattice is populated, so $[\mathrm{B}]=[\mathrm{B}_+]/2$ (=0.425 34, from above) and $[\mathrm{B}_-]=0$. Furthermore, this value of [B] can be readily estimated noting that there must be a steady-state balance between the *creation* of defects due to removal of monomer B's, and the *removal* of defects via subsequent immediate deposition of dimer B_2's according to the eight-site rule. In fact, for each monomer removed, there must be a

probability for dimer adsorption of 1/2. Thus, the probability for lack of dimer adsorption must also equal 1/2. The latter quantity is given by the conditional probability Q_+ that all four of the sites diagonally adjacent to a specific B_+ (which is to be removed by reaction) are occupied by B_+, thus prohibiting dimer adsorption. Consequently, we conclude that[30]

$$Q_+ = \begin{bmatrix} B_+ & & B_+ \\ & B_+ & \\ B_+ & & B_+ \end{bmatrix} / [B_+] = 1/2. \tag{12}$$

Next, we estimate Q_+ with various assumptions regarding the B adlayer structure on the populated + sublattice. First, we present the simplest analysis, which results from assuming that the defects or holes are randomly distributed on the + sublattice. Then, it follows that

$$Q_+ \approx [B_+]^4 = 2^4[B]^4 = 1/2, \tag{13}$$

so $[B] \approx 2^{-5/4} \approx 0.4204$ in the steady state. Second, we note that distribution of defects on the + sublattice must be correlated in any jammed state of the adlayer, since no two defects or holes can be on adjacent sublattice sites (i.e., on diagonal NN sites of the square lattice of adsorption sites). Adopting a pair-type approximation, and exploiting the above observation, one obtains

$$\begin{aligned} Q_+ &\approx \begin{bmatrix} & B_+ \\ B_+ & \end{bmatrix}^4 / [B_+]^4 \\ &= (2[B_+] - 1)^4 / [B_+]^4 \\ &= (4[B] - 1)^4 / (2[B]^4) = 1/2, \end{aligned} \tag{14}$$

so $[B] \approx (4 - 2^{3/4})^{-1} \approx 0.4314$ in the steady state. Both these simple estimates are reasonably close to the exact simulation result of $[B] = 0.425\,34$. A framework within which more sophisticated determination can be made of this steady-state coverage is provided by the analytic formalism described at the end of Sec. V B for B dynamics on a sublattice.[30]

VI. SUMMARY

In this paper, we have analyzed the steady-state properties of a new ''canonical'' lattice–gas model for CO oxidation which incorporates superlattice ordering of O(ads), as well as rapid mobility of CO(ads). (Here, we revert to physical terminology, rather than using $A + B_2$ notation.) As might be expected given the Langmuir–Hinshelwood mechanism for this reaction, the steady states exhibit bistability, a feature which is lost at a cusp bifurcation or ''critical point'' when the desorption rate d for CO(ads) exceeds a critical value. In Ref. 12, we have shown that behavior near this point is analogous to that near critical points in equilibrium Hamiltonian systems, e.g., fluctuations in coverages are enhanced. The model also exhibits a symmetry-breaking order–disorder transition in the oxygen adlayer when its coverage exceeds a value of about 0.29. This behavior is analogous to order–disorder transitions in equilibrium systems such as the hard-square model.[18] This order–disorder transition replaces the unphysical (continuous) oxygen poisoning transition common in previous lattice–gas models for CO oxidation without superlattice ordering.[4,16] Coarsening phenomena are also observed in our new model associated with symmetry breaking, reminiscent of Lifshitz–Cahn–Allen coarsening in Hamiltonian systems. We mention that analogous behavior has been observed as a result of introducing relaxation processes into irreversible RSA models.[31,32]

We have emphasized in Sec. I that our model is still rather simplistic. To precisely describe behavior in actual systems, more realistic and complicated reaction models must be utilized. These should incorporate, e.g., CO(ads)–CO(ads) and CO(ads)–O(ads) interactions, in addition to strongly repulsive short-range O(ads)–O(ads) interactions, and possibly also some diffusion of O(ads). Reference 17 includes some of these features. Both symmetry breaking and coarsening driven by the strong short-range repulsions will no doubt persist in these more realistic models.

ACKNOWLEDGMENTS

The authors wish to acknowledge valuable discussions with Da-Jiang Liu. They have also benefitted from collaborative studies with R. Imbihl and Y. Suchorski on critical behavior in catalytic CO oxidation. This work was supported by the Division of Chemical Sciences, Office of Basic Energy Sciences, of the U.S. Department of Energy (USDOE). It was performed at Ames Laboratory, which is operated for the USDOE by Iowa State University under Contract No. W-7405-Eng-82.

APPENDIX A: THE PAIR APPROXIMATION

Substituting Eqs. (5)–(7) into the steady-state form of Eq. (4b) yields an 11th-order polynomial equation

$$\begin{aligned} &2P_{B_2}(1-2[B])^8\{4k[B] + d(1-[B])\}^2 - 4kP_A[B] \\ &\times (1-[B])^9\{(P_A + d)(1-[B]) + 4k[B]\} = 0 \end{aligned} \tag{A1}$$

to be solved for the steady-state values of $[B]$. Corresponding steady-state $[A]$ values then follow immediately from Eq. (7). We emphasize that analysis of Eq. (A1) yields estimates of both the (two) stable and (one) unstable steady states, the remaining eight solutions being unphysical. As a specific example, we note that the limiting behavior in the reactive state when $P_A \to 0$ can be analyzed directly (although not accurately) from Eq. (A1). Specifically, one obtains

$$(1-2[B])^8 \sim cP_A, \quad \text{so } [B] \sim 1/2 - \tfrac{1}{2}c^{1/8}(P_A)^{1/8}, \tag{A2}$$

as $P_A \to 0$, where $c = 2^{-10}4k/(4k+d)$.

APPENDIX B: CHEMICAL WAVES AND RELATIVE STABILITY

Relative stability of coexisting stable states in reaction models is naturally defined in terms of the motion of planar chemical waves which separate these states: the more stable state should displace the less stable one. To apply this paradigm to our model, it is necessary to regard the hop rate(s) for A as finite but very large, rather than being strictly infinite. Then, in spatially localized regions of the surface, the A's are randomized with a uniform coverage. However, spatial variations in coverage can occur on a macroscopic length

scale controlled by the diffusivity of A. For simplicity, let us denote the RHS of Eq. (4a) by R_A, and of Eq. (4b) by R_B. Then, chemical waves are described by the reaction-diffusion equations

$$d/dt\ [A]=R_A-\nabla\cdot\mathbf{J}_A$$

and

$$d/dt\ [B]=R_B, \tag{B1}$$

where

$$\mathbf{J}_A=-D_{A,A}\nabla[A]-D_{A,B}\nabla[B].$$

Here, ∇ denotes ''grad'' or ''div'' in the surface plane. The diffusive flux, $\mathbf{J}_A$, of A includes a conventional term proportional to $\nabla[A]$, as well as a typically neglected term proportional to $\nabla[B]$.[3,8] The $D_{A,K}$ with $K=$A or B denote entries in a tensor of diffusion coefficients. Note that $\mathbf{J}_B=0$ since B is immobile. $D_{A,A}$ and $D_{A,B}$ have the specific form (see Ref. 8)

$$D_{A,A}=D_0F(\{B\}),$$

and

$$D_{A,B}=D_0[A]F(\{B\})/(1-[B]), \tag{B2}$$

where {B} denotes the configuration of the B adlayer. The function $F(\{B\})$ is unity for $[B]=0$, and decreases with increasing [B] due to the blocking effect of B on A diffusion. General analysis of chemical waves requires detailed characterization of $F(\{B\})$, which constitutes a nontrivial problem in transport in disordered systems.[33] However, near the cusp bifurcation, coexisting stable states become indistinguishable (with $[B]\to0.033$ and $[A]\to0.633$), as do all states across the chemical wave front. Thus, in this regime, chemical wave propagation and relative stability can be analyzed treating $D_{A,A}$ and $D_{A,B}$ in Eq. (B1) as constants with $D_{A,B}/D_{A,A}\approx0.65$.

APPENDIX C: STEADY-STATE BEHAVIOR FOR $k\ll1$ AND $k\gg1$

First, consider the case $k\ll1$, where the overall process is reaction limited. The steady-state relation, Eq. (7), shows immediately that $[A]\approx P_A(P_A+d)^{-1}(1-[B])$. For $d=0$, we argued in Sec. IV B that $[A]=1$ and $[B]=0$. For $d>0$, one has $[A]+[B]<1$, even in the steady state. Thus, in general B_2 adsorption is possible and, since B removal by reaction occurs on a much slower time scale, adsorption will continue until the system reaches a jammed state. It is clear that this jammed state is actually independent of P_A, and coincides with that analyzed for $k=1$ when $P_A\to0+$, so $[B]=0.425\,34$.

Second, consider the case $k\to\infty$ (instantaneous reaction), where the overall process is adsorption limited. Rapid reaction, together with the infinite diffusion rate for A in our hybrid model, implies that only one type of species can populate the surface.[9,17,25] If the populating species is A, so $[A]>0$ and $[B]=0$ (corresponding to a relatively inactive state), then A is randomly distributed, and as a result B_2 adsorbs at rate $2P_{B_2}(1-[A])^2$ and immediately reacts. Thus, one has

$$d/dt\ [A]=P_A(1-[A])-d[A]-2P_{B_2}(1-[A])^2, \tag{C1}$$

just as in the monomer–dimer model with B_2 adsorption on adjacent sites (for infinite diffusivity of A, and $k\to\infty$).[25] From Eq. (C1), it follows that the lower and upper spinodals satisfy $P^-(d)=(24d^2+8d)^{1/2}-5d$ and $P^+(d)=2/3$, respectively, for $d<d_c=2/3$.[9,25]

If the populating species is B, so $[B]>0$ and $[A]=0$ (corresponding to the reactive state), then A adsorbs at rate $P_A(1-[B])=P_A[Z]$, and reacts immediately removing a B. Thus, one has

$$d/dt\ [B]=2P_{B_2}\begin{bmatrix} & & Z & \\ & Z & Z & Z \\ Z & Z & Z & \\ & Z & & \end{bmatrix}-P_A[Z]. \tag{C2}$$

This is the first equation in a hierarchy, which can only be solved with further approximation to achieve closure. Note that this B populated reactive state is independent of d. The steady-state value of [B] equals 0.3616 if $P_A=0$ (RSA), but then jumps to 0.425 34 for $P_A=0+$, and then decreases to 0, as P_A increases from 0+ to 2/3 (cf. Sec. IV B). Finally, we note that it is natural to view this reaction model as a single species model involving B_2 dimer adsorption and B monomer desorption. Dimer adsorption occurs according to the eight-site rule with an impingement rate of P_{B_2} per site. Monomer desorption occurs randomly at a rate of $P_A(1-[B])$ per site.

[1] R. Imbihl and G. Ertl, Chem. Rev. **95**, 697 (1995).
[2] J. Wintterlin, S. Volkening, T. V. W. Janssens, T. Zambelli, and G. Ertl, Science **278**, 1931 (1997).
[3] M. Tammaro and J. W. Evans, Surf. Sci. Lett. **395**, L207 (1998).
[4] E. V. Albano, Heterog. Chem. Rev. **3**, 389 (1996); J. W. Evans and M. Sabella, Trends Stat. Phys. **1**, 107 (1994); V. P. Zhdanov and B. Kasemo, Surf. Sci. Rep. **20**, 111 (1994); J. W. Evans, Langmuir **7**, 2514 (1991).
[5] W. H. Weinberg, Annu. Rev. Phys. Chem. **34**, 217 (1983); K. Binder and D. P. Landau, Adv. Chem. Phys. **26**, 91 (1989).
[6] J. W. Evans and T. R. Ray, Phys. Rev. E **50**, 4302 (1994).
[7] M. Tammaro, M. Sabella, and J. W. Evans, J. Chem. Phys. **103**, 10277 (1995).
[8] M. Tammaro and J. W. Evans, J. Chem. Phys. **108**, 762 (1998).
[9] J. W. Evans and M. Tammaro, in *Computer Simulation Studies in Condensed Matter Physics XI*, edited by D. P. Landau and H. B. Schuettler (Springer, Berlin, 1998), pp. 103–117; M. Tammaro and J. W. Evans, Phys. Rev. E **57**, 5087 (1998).
[10] M. Silverberg and A. Ben-Shaul, J. Chem. Phys. **87**, 3178 (1989); H. C. Kang, T. A. Jachimowiski, and W. H. Weinberg, J. Chem. Phys. **93**, 1418 (1990).
[11] G. A. Somorjai, *Introduction to Surface Chemistry and Catalysis* (Wiley, New York, 1994).
[12] Y. Suchorski, J. Beben, E. W. James, J. W. Evans, and R. Imbihl, Phys. Rev. Lett. **82**, 1907 (1999).
[13] C. R. Brundle, R. J. Behm, and J. A. Barker, J. Vac. Sci. Technol. A **2**, 1038 (1984).
[14] S.-L. Chang and P. A. Thiel, Phys. Rev. Lett. **59**, 296 (1987); S.-L. Chang, D. E. Sanders, J. W. Evans, and P. A. Thiel, in *The Structure of Surfaces II*, Proceedings of ICSOS II, edited by J. F. van der Veen and M. A. Van Hove (Springer, Berlin, 1988), pp. 231–237.
[15] J. W. Evans, J. Chem. Phys. **87**, 3038 (1987); J. W. Evans and D. E. Sanders, Phys. Rev. B **39**, 1587 (1989).
[16] R. M. Ziff, E. Gulari, and Y. Barshad, Phys. Rev. Lett. **56**, 2553 (1986).
[17] V. P. Zhdanov and B. Kasemo, Surf. Sci. **412/413**, 527 (1998).
[18] F. H. Ree and D. A. Chesnut, J. Chem. Phys. **45**, 3983 (1966).
[19] J. W. Evans, Rev. Mod. Phys. **65**, 1281 (1993).
[20] The density of ''internal defects'' or ''holes,'' H, in $c(2\times2)$ domains is

given by

$$[H]=\begin{bmatrix} B & & B \\ & Z & \\ B & & B \end{bmatrix}=\begin{bmatrix} B & Z & B \\ Z & Z & Z \\ B & Z & B \end{bmatrix}.$$

[21] Lattice–gas reaction models with finite adspecies hop rates can have only one true stable steady state, perhaps coexisting with a metastable steady state with a finite lifetime.

[22] R. M. Ziff and B. J. Brosilow, Phys. Rev. A **46**, 4630 (1992).

[23] E. W. James, D.-J. Liu, and J. W. Evans (unpublished).

[24] If only *one* sublattice is populated, except for randomly distributed ''defects,'' then the probability on the LHS of Eq. (6) equals the average of $(1-[A]-2[B])^2$ and $(1-[A])^2(1-2[B])^6$. These terms correspond to choosing the central empty sites on the B-populated and B-unpopulated sublattices, respectively. The result differs from that obtained via Eq. (9), but is still inaccurate.

[25] J. W. Evans, J. Chem. Phys. **98**, 2463 (1993).

[26] S. M. Allen and J. W. Cahn, Acta Metall. **27**, 1085 (1979); I. M. Lifshitz, Sov. Phys. JETP **15**, 939 (1962).

[27] M. A. Van Hove, W. H. Weinberg, and C.-M. Chan, *Low-Energy Electron Diffraction* (Springer, Berlin, 1986).

[28] A.-L. Barabasi and H. E. Stanley, *Fractal Concepts in Surface Growth* (Cambridge University Press, Cambridge, 1995).

[29] R. H. Goodman, D. S. Graff, L. M. Sander, P. Lerox-Hugon, and E. Clement, Phys. Rev. E **52**, 5904 (1995); H. C. Kang and W. H. Weinberg, *ibid.* **47**, 1604 (1993); **48**, 3464 (1994).

[30] Let Q_+ denote the probability that a dimer does *not* adsorb when a B_+ is removed from the + sublattice (cf. Sec. V C). Then, the rate of loss of B_+ due to monomer desorption equals $Q_+[B_+]$, and the rate of gain due to dimer adsorption equals $(1-Q_+)[B_+]$. Thus, one has $d/dt'\ [B_+]=(1-Q_+)[B_+]-Q_+[B_+]=(1-2Q_+)[B_+]$. This is the lowest order equation in an exact hierarchy.

[31] V. Privman, in *Annual Reviews of Computational Physics III*, edited by D. Stauffer (World Scientific, Singapore, 1995).

[32] E. W. James, D.-J. Liu, and J. W. Evans, Colloids Surf. A (to be published).

[33] D.-J. Liu and J. W. Evans, Bull. Am. Phys. Soc. **44**, 1387 (1999).